AMERICAN SOCIETY FOR MICROBIOLOGY | Antimicrobial Agents and Chemotherapy

Check for updates

| Antimicrobial Chemotherapy | Full-Length Text

Pharmacokinetic-pharmacodynamic modeling to evaluate the relative impact of immune response and meropenem on bacterial killing *in vivo*

Raphaël Saporta,[1] Natália Tassi,[2] Veronica Biordi,[2] Olga Ticha,[2] Aghavni Ginosyan,[1] Irena Loryan,[1] Elisabet I. Nielsen,[1] Isabelle Bekeredjian-Ding,[2] Bernhard Kerscher,[2] Lena E. Friberg[1]

AUTHOR AFFILIATIONS See affiliation list on p. 12.

ABSTRACT *In vivo* antibiotic pharmacokinetic-pharmacodynamic (PKPD) properties are typically studied in neutropenic infection models, limiting the understanding of interactions between immune cells and antibiotics. This study aimed to characterize the impact of immune status on meropenem PKPD and dose-response in a mouse lung infection model, and to quantify the relative contribution of immune response and meropenem to bacterial killing. Meropenem PK was analyzed in plasma and epithelial lung fluid, and bacterial counts were monitored over 24 h following 40 or 300 mg/kg meropenem doses every 4 h in a mouse lung infection model with varying immunosuppression levels (neutropenic, intermediate, or immunocompetent). A PKPD model was developed to quantify bacterial killing by the immune response and meropenem over time. Dose-fractionation studies were simulated to investigate meropenem dose-response in different immune states. Observed differences in meropenem concentration-time profiles were explained by a higher volume of distribution in immunocompetent mice. The immune response was described by phagocytosis and digestion processes. The meropenem effect was best quantified based on plasma concentrations, with a maximal killing rate of 0.934 h^{-1} and EC_{50} = 1.62 mg/L. The lower contribution of meropenem to bacterial killing in intermediate and immunocompetent conditions was explained as a lower fraction of bacteria being affected by meropenem. In simulations, the immune status impacted PKPD target derivation. The developed model characterized differences in meropenem PK between neutropenic and immunocompetent *in vivo* infection models and quantified the contributions of immune response and meropenem to bacterial killing, with a reduced effect of meropenem in immunocompetent systems.

KEYWORDS meropenem, immune response, modeling, pharmacokinetics-pharmacodynamics

Despite the importance of the immune response in infection control, its quantitative contribution to bacterial killing, particularly in the presence of antibiotics, is not fully understood. The innate immune response involves mechanisms to control and eliminate pathogens (1). Neutrophils, the most abundant circulating white blood cells in humans, employ different processes to induce bacterial killing, such as the phagocytosis of bacteria followed by the release of antibacterial proteins into the formed phagosome, degranulation, or the formation of neutrophil extracellular traps (2). The critical role of neutrophils is evidenced in patients with neutropenia (an absolute neutrophil count below 1.5 × 10^9/L (3)), which is associated with an increased infection risk and mortality (4).

Editor James E. Leggett, Providence Portland Medical Center, Portland, Oregon, USA

Address correspondence to Lena E. Friberg, lena.friberg@uu.se.

The authors declare no conflict of interest.

See the funding table on p. 13.

Received 24 November 2025
Accepted 15 January 2026
Published 20 February 2026

Copyright © 2026 Saporta et al. This is an open-access article distributed under the terms of the Creative Commons Attribution 4.0 International license.

Downloaded from https://journals.asm.org/journal/aac on 17 August 2026 by 130.238.171.108.

Downloaded from https://journals.asm.org/journal/aac on 17 August 2026 by 130.238.171.108.

Although the immune response is crucial, it may not always be sufficient. Antibiotics, such as the carbapenem meropenem, are essential in the treatment of bacterial infections in clinical practice. During antibiotic drug development and regulatory evaluation, animal infection models are key in the pharmacokinetic-pharmacodynamic (PKPD) characterization (5, 6), with the neutropenic mouse thigh and lung infection models being most common (7). Neutropenia, usually induced by administering cyclophosphamide, allows sustained immunosuppression over the study duration (8, 9). The antibiotic PKPD is, therefore, characterized under conditions that limit the confounding of drug effects with immune response. Additionally, more strains can successfully grow in neutropenic conditions. However, varying degrees of immune response are expected in clinical practice, yet these preclinical models neither quantify immune-related bacterial killing nor evaluate potential interplays between the immune system and the antibiotic's PKPD properties.

PKPD modeling has been increasingly employed to characterize the time course of antibiotic effects, based on *in vitro* and/or *in vivo* data (10–12). However, few studies have quantified the impact of immunosuppression on bacterial killing (13–16), and models addressing both drug effect and immune response are particularly scarce (17, 18).

The PKPD of meropenem has been extensively studied under both *in vitro* and neutropenic *in vivo* conditions, including through PKPD modeling (19, 20). However, despite the importance of carbapenems in clinical practice (21), little is known about how the PKPD of meropenem is dependent on immunocompetent conditions. This study aimed to characterize meropenem PK and PKPD in neutropenic and immunocompetent conditions by quantifying the relative contributions of meropenem and the immune system to bacterial killing in a mouse lung infection model using PKPD modeling, and to explore the impact of the immune system on meropenem dose-response and derived PKPD targets through simulations.

MATERIALS AND METHODS

Mouse lung infection model

Specific pathogen-free CD-1 female mice (Janvier Labs, France) of 6–10 weeks of age at intervention start were used, in line with a standardized murine lung infection model, the COMBINE pneumonia model (9), with modifications to the standard model regarding the immune status. Two different intraperitoneal dosing regimens of cyclophosphamide (Baxter, Germany) were used to induce different states of immunosuppression in mice: the intermediate state was obtained with 75 and 50 mg/kg intraperitoneal doses at 4 and 1 days before infection, respectively, and the neutropenic state with 200 and 150 mg/kg intraperitoneal doses at the same time points. For the immunocompetent state, no cyclophosphamide was administered.

Klebsiella pneumoniae DSM116099 was obtained from the German culture collection DSMZ (Leibniz Institute, Germany). Meropenem minimum inhibitory concentration (MIC) was identified at 0.032 mg/L by determination in triplicate by microdilution broth according to the EUCAST guidelines (22). On the day of infection, bacteria were inoculated into fresh tryptic soy broth media from an overnight culture, grown to logarithmic phase, washed with phosphate-buffered saline (PBS) twice, and resuspended in PBS to the desired concentration, based on individually established correlation curves. Mice were anesthetized with 3.5% isoflurane in oxygen-enriched air, and bacterial suspensions were applied intranasally by depositing 50 µL of suspension into the nares and allowing the mice to inhale.

Meropenem (Inresa Arzneimittel GmbH, Germany) was administered subcutaneously based on individual animal weights. For PK experiments, a single dose of 40 or 300 mg/kg was given at 2 h post-infection. For PD experiments, doses of 40 or 300 mg/kg were given every 4 h, starting at 2 h post-infection.

Mice were euthanized by CO_2 or anesthetics overdose followed by cervical dislocation when reaching the humane endpoint/severity limit or at the study endpoint. In PK (n =

60 mice) and PD (n = 180 mice) experiments, blood, bronchoalveolar lavage (BAL), and whole lung tissue samples were taken at times detailed in Table S1.

Sampling and analyses

In PK experiments, plasma samples were collected in EDTA tubes from superficial veins or by cardiac puncture under terminal FDA ketamine-xylazine anesthesia. Total meropenem concentration in plasma and BAL samples was quantified using Acquity ultra-performance liquid chromatography coupled with Xevo TQ-S Micro triple quadrupole mass spectrometer (UPLC-MS/MS, Waters Corporation, Milford, MA, USA). Data acquisition and quantitation were done using Masslynx v4.2 (Waters Corporation). The method for the assessment of plasma concentrations was developed based on previously published protocols with modifications (23–25). The bioanalytical method was validated for selectivity, response function, range, intra- and inter-day accuracy, precision, matrix effect, and carryover according to the FDA guidance (26). The lowest standard concentration (0.05 mg/L) was set as the lower limit of quantification (LLOQ) in plasma and BAL. Meropenem concentrations in epithelial lining fluid (ELF) were derived from meropenem concentrations in BAL by urea correction ($C_{ELF} = C_{BAL} \times Urea_{plasma}/Urea_{BAL}$).

In PD experiments, general blood cell counts were determined by a veterinary clinical blood analyzer (scil animal care company GmbH, Germany). For CFU enumeration, right lungs were collected in Lysing Matrix D (MP Biomedicals, Germany) containing 1 mL of 0.1% Triton X-100 (Sigma-Aldrich, Germany) in PBS. The tissue homogenate was generated by three cycles of bead-beating (5,000 rpm, 13 s/cycle with 15-s breaks) on a Pracellys 24 touch (Bertin Technologies, Germany). Serial dilutions in PBS were prepared in duplicate. Dilutions 10^{-1} to 10^{-8} were plated on tryptic soy agar and incubated at 37°C overnight.

PK modeling

Compartmental models were investigated to describe meropenem plasma and lung (ELF) concentrations. Absorption following subcutaneous (SC) drug administration was evaluated as a first- or zero-order process. Potential differences in PK parameters between immunocompetent and neutropenic mice were assessed.

PKPD modeling

The PKPD model structure was developed in two steps. First, data from control groups (without antibiotic treatment) were analyzed alone to develop the model structure for bacterial growth and immune response. Second, data from treatment groups were incorporated, and all data were analyzed simultaneously to characterize the meropenem effect.

Bacteria were described to be in a growing and drug-susceptible (S) state, or in a dormant (or resting), non-growing and non-drug-susceptible (D) state (27). Bacterial growth was defined by a rate constant k_{growth}. In both states, a non-immune-related natural death rate constant k_{death} was implemented. The rate constant for transfer from S to D, k_{SD}, was linked to the current total bacterial count and the maximum system capacity, B_{max}, with $k_{SD} = (S + D)\cdot(k_{growth} - k_{death})/B_{max}$. For each immune state, the S compartment was initialized to the median bacterial count from control groups at 2 h after infection. The immune response was described as a phagocytosis and digestion process (16). Bacteria in the S and D states transferred to a third bacterial state, phagocytosis (P), at a rate k_{phag}, followed by their digestion and removal from the system at a rate k_{dig}. Bacteria in the P state were also assumed to contribute to the total CFU counts but not to B_{max}, as phagocytic cells were lysed prior to the counting procedure.

The rates k_{phag} and k_{dig} were assessed to be dependent on immune status, either as condition-specific parameters or by assuming they were related to blood or lung granulocyte counts. Granulocyte recruitment to the infection site was investigated either through a function for a time-dependent increase in k_{phag}, an effect compartment, or

Downloaded from https://journals.asm.org/journal/aac on 17 August 2026 by 130.238.171.108.

a surge function for granulocyte recruitment to the lungs using previously estimated parameters (16). As the killing rate attributable to granulocytes was previously shown to be subject to saturation at high bacterial burdens (14–16), functions were explored to describe a reduced phagocytic activity with increasing P bacteria compared to the number of available granulocytes.

The meropenem effect was implemented as an additional bacterial killing rate, k_{drug}, on bacteria in the S state. Bacterial dynamics were described by the following equations:

$$\frac{dS}{dt} = k_{growth} \cdot S - \left(k_{death} + k_{drug}\right) \cdot S - k_{SD} \cdot S - k_{phag} \cdot S \quad (1)$$

$$\frac{dD}{dt} = k_{SD} \cdot S - k_{death} \cdot D - k_{phag} \cdot D \quad (2)$$

$$\frac{dP}{dt} = k_{phag} \cdot S + k_{phag} \cdot D - k_{dig} \cdot P \quad (3)$$

Unbound meropenem plasma (fu = 0.81) (19) or ELF concentrations predicted from the PK model were used to drive the drug effect. Meropenem effect was evaluated with slope or power ($\gamma = 1$ or $\gamma \neq 1$, equation 4), E_{max} or sigmoid E_{max} ($\gamma = 1$ or $\gamma \neq 1$, equation 5) models:

$$k_{drug} = \text{Slope} \cdot C^{\gamma} \quad (4)$$

$$k_{drug} = \frac{E_{max} \cdot C^{\gamma}}{EC_{50}^{\gamma} + C^{\gamma}} \quad (5)$$

where C is the unbound meropenem concentration, Slope is the drug effect slope, E_{max} is the maximum drug effect, EC_{50} is the meropenem concentration at which 50% of E_{max} is reached, and γ is the power or sigmoidicity parameter. Drug effect parameters were estimated simultaneously with other PD parameters. The possibility that meropenem affects P bacteria was also evaluated.

Simulation of dose-ranging and dose-fractionation studies

The final PKPD model was used to predict response in meropenem studies in a mouse lung infection model in neutropenic, intermediate suppression, and immunocompetent conditions. All simulations were performed considering an inoculum of 7.5 $\log_{10}$ CFU/lung, and without residual variability. A dose-ranging study with doses ranging from 20 to 1,200 mg/kg administered every 4 h, and a dose-fractionation study with total doses equivalent to those of the 40 and 300 mg/kg every 4 h regimens, fractionated in administrations every 2, 4, 6, or 8 h, were simulated to explore the predicted bacterial dynamics over 24 h of treatment. Additionally, a dose-fractionation study was simulated based on a literature design (28), with a start of treatment 2 h after inoculation. Simulated bacterial counts at 26 h (24 h after start of treatment) were correlated to derived PK/PD indices: the unbound maximum concentration (fC_{max}) to MIC ratio (fC_{max}/MIC), the area under the unbound concentration-time profile curve (fAUC) to MIC ratio (fAUC/MIC), and the fraction of time unbound concentrations exceeded the MIC ($fT_{>MIC}$). The relationship between 26-h bacterial counts and PK/PD indices was evaluated with a sigmoid E_{max} function:

$$E = E_0 - \frac{PD_{max} \cdot \text{Index}^{H}}{\text{Index}_{50}^{H} + \text{Index}^{H}} \quad (6)$$

where E is the 26-h bacterial load, E_0 is the 26-h bacterial load when Index = 0, PD_{max} is the maximum reduction in bacterial load from E_0 after 24 h of treatment, H is the Hill factor for sigmoidal shape, Index is the PK/PD index value, and $Index_{50}$ is the PK/PD index value required to reach half of PD_{max}. Correlations between simulated bacterial counts and fitted E_{max} curves were computed (R^2 values).

Downloaded from https://journals.asm.org/journal/aac on 17 August 2026 by 130.238.171.108.

Downloaded from https://journals.asm.org/journal/aac on 17 August 2026 by 130.238.171.108.

Data analysis and software

Model development was performed in NONMEM 7.5.0 (29), assisted by Perl-speaks-NONMEM version 5.2.6 (30), using the Laplacian conditional estimation method with interaction. PK modeling was performed using a log-transform-both-sides approach, and data below the LLOQ were handled using the M3 method (31). A $\log_{10}$-transform-both-sides approach was used for PKPD modeling. Residual errors were described by additive terms on the log-transformed scales. The difference in the objective function value (ΔOFV) was used to evaluate parameter inclusion, with a decrease in OFV of 3.84 points considered statistically significant for the inclusion of one extra parameter (α = 0.05). Other model selection criteria were scientific plausibility, parameter uncertainty as estimated using sampling importance resampling (32), and goodness-of-fit plots including simulation-based visual predictive checks (VPCs) (33). Data management and graphical analysis were conducted in R version 4.3.3 (34). Simulations were carried out in NONMEM 7.5.0 and in R using mrgsolve version 1.5.1 (35). Curve fitting for PK/PD indices was performed using drc version 3.0-1 in R (36).

RESULTS

Mouse PK experiments and PK modeling

Meropenem plasma PK following SC administration was captured by a one-compartment model, with first-order absorption, while lung concentrations in ELF were described by a two-compartment model. Mass transfer between plasma and lung compartments was not retained in the model to improve stability and provide reliable plasma predictions. Differences in plasma and ELF concentration-time profiles were observed between neutropenic and immunocompetent mice, best described by different central volumes of distribution, with a central volume of 2.19 and 3.40 L/kg for neutropenic and immunocompetent mice, respectively (ΔOFV = −29.4 compared to a model in which the same volume of distribution was shared between both immune

TABLE 1 Parameter estimates and relative standard errors (RSEs) of the final model in neutropenic, intermediate suppression, or immunocompetent mice

Parameter	Unit	Description	Estimate	RSE (%)
CL	L/(h·kg)	Apparent clearance	5.33	11
V_{neu}	L/kg	Apparent central volume of distribution (neutropenic)	2.19	18
V_{int}	L/kg	Apparent central volume of distribution (intermediate suppression)	2.46[a]	Fixed
V_{com}	L/kg	Apparent central volume of distribution (competent)	3.4	18
k_a	h^{-1}	Absorption rate constant	71.3	39
V_{ELF}	L/kg	Apparent ELF volume of distribution	0.0554	23
V_{L2}	L/kg	Apparent volume of distribution of second lung compartment	9.27	26
Q	L/(h·kg)	Apparent intercompartmental clearance (central-ELF)	0.385	19
Q_2	L/(h·kg)	Apparent intercompartmental clearance (ELF-lung)	2.48	13
k_{growth}	h^{-1}	Bacterial growth rate constant	0.372	11
k_{death}	h^{-1}	Bacterial natural death rate constant	0.179[a]	Fixed
B_{max}	$\log_{10}$ CFU/lung	Maximum bacterial count	9.59[a]	Fixed
IR_{neu}	h^{-1}	Phagocytosis rate (k_{phag}) in neutropenic state $k_{phag} = IR_{neu}$	0[a]	Fixed
IR_{int}	h^{-1}	Increase in phagocytosis rate in intermediate suppression state $k_{phag} = IR_{neu} + IR_{int}$	0.185	12
IR_{com}	h^{-1}	Increase in phagocytosis rate in immunocompetent state $k_{phag} = IR_{neu} + IR_{int} + IR_{com}$	0.133	18
E_{max}	h^{-1}	Maximum meropenem effect (killing rate constant)	0.934	14
EC_{50}	mg/L	Concentration needed to achieve 50% of E_{max}	1.62	18
RES_{Plasma}	–	Residual error of ELF PK (standard deviation)	0.816	17
RES_{ELF}	–	Residual error of plasma PK (standard deviation)	0.738	22
RES_{PD}	$\log_{10}$ CFU/lung	Residual error of the PKPD model (standard deviation)	0.623	14

[a]Fixed parameters.

states). In the PKPD modeling, the meropenem central volume of distribution in mice with intermediate suppression was scaled to 2.46 L/kg by linear interpolation based on median white blood cell counts from the PD experiments. Parameters were estimated with acceptable precision (relative standard errors [RSE] < 40%, Table 1). VPCs suggested a good description of plasma and ELF concentrations for both dose groups and both immune states (Fig. 1).

Mouse PD experiments and PKPD modeling

Median observed bacterial counts at 2 h after infection were 7.56, 7.80, and 7.52 $\log_{10}$ CFU/lung for neutropenic, intermediate, and competent groups, respectively. Small to no time trends were observed in white blood cell and blood granulocyte counts (Fig. S1 and S2, observed cell type distribution presented in Table S2. Consequently, modeling of granulocyte blood dynamics was not explored, but median granulocyte counts (0.2×10^3, 0.4×10^3, and 1.9×10^3/mm^3 in neutropenic, intermediate, and immunocompetent states, respectively) were investigated to scale k_{phag} and/or k_{dig}. This led to a worse model fit compared to using the immune status as a categorical covariate. The structure of the final model is presented in Fig. 2, with parameter estimates and associated uncertainties in Table 1. As no bacterial plateau phase was visible in control groups, B_{max} could not be reliably estimated (high standard errors and/or non-plausible estimates) and was, thus, fixed to the median bacterial count in neutropenic controls at

Downloaded from https://journals.asm.org/journal/aac on 17 August 2026 by 130.238.171.108.

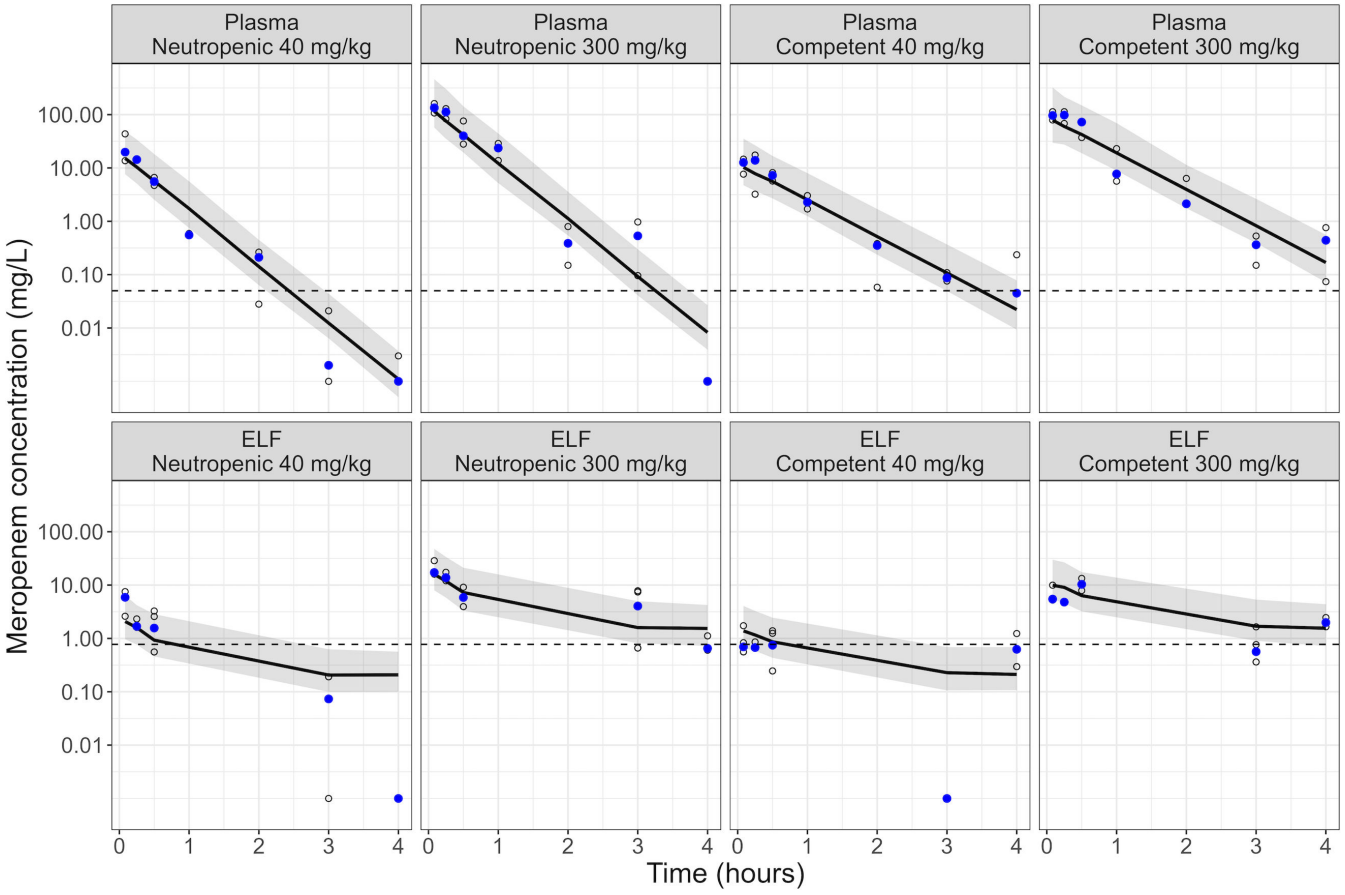

FIG 1 VPCs of the final PK model. Shown are the observed (open circles) and median of observed (solid blue circles) meropenem concentrations, the median (solid line) and the 95% confidence interval of the median (shaded area) of model predictions in plasma and ELF for the meropenem doses in neutropenic and immunocompetent mice. The lower limit of quantification is indicated by the horizontal dashed line, with the lower limit of quantification in ELF derived based on urea correction from the limit of quantification in BAL. Observations below the limit of quantification are displayed at their measured (plasma) or derived (ELF) value.

Downloaded from https://journals.asm.org/journal/aac on 17 August 2026 by 130.238.171.108.

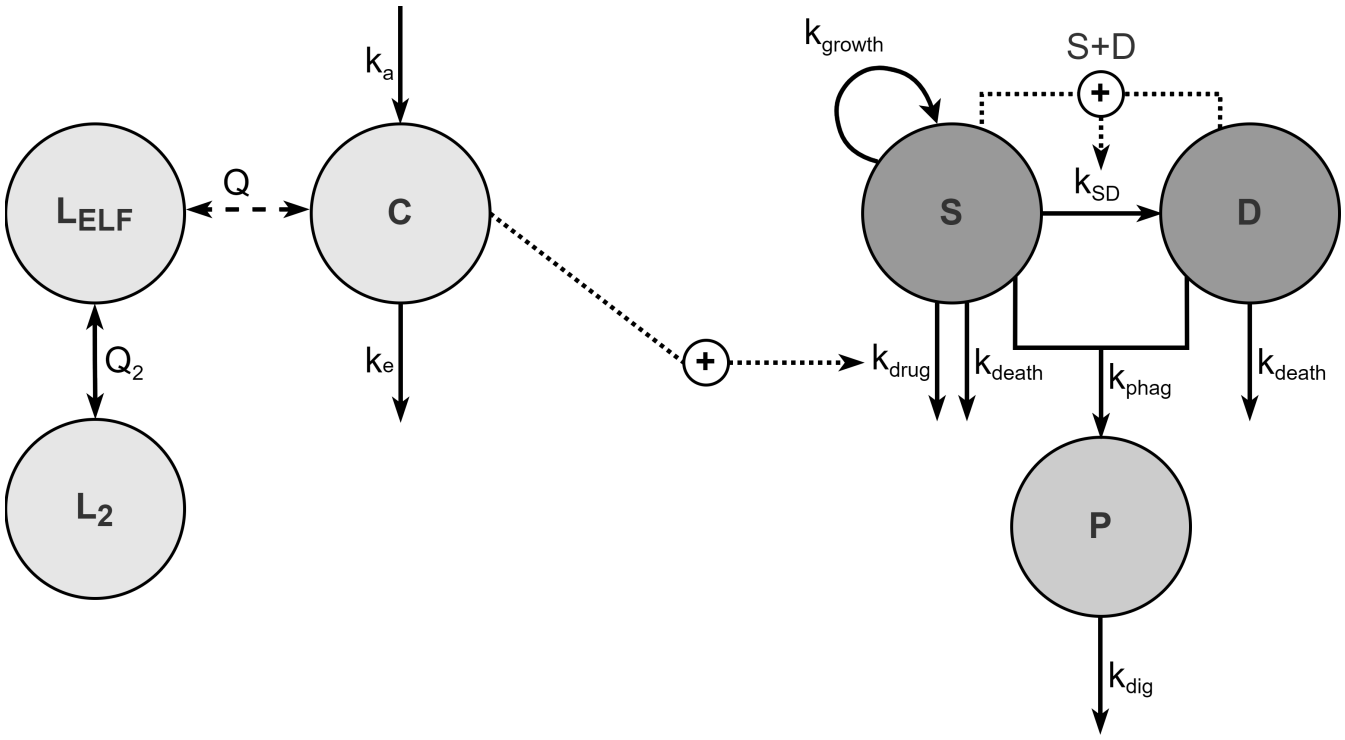

FIG 2 Schematic representation of the final PKPD model. C, meropenem plasma concentration. D, dormant bacteria. k_a, absorption rate constant. k_{death}, bacterial natural death rate constant. k_{dig}, digestion rate constant. k_{drug}, meropenem effect rate constant. k_e, elimination rate constant. k_{growth}, bacterial growth rate constant. k_{phag}, phagocytosis rate constant. k_{SD}, transfer from susceptible to dormant state rate constant. L_{ELF}, meropenem ELF compartment. L_2, meropenem second lung compartment. P, phagocytosed bacteria. S, susceptible bacteria. Q and Q_2, intercompartmental clearances.

26 hours after infection. A saturation of the immune response, or functions describing the recruitment of granulocytes to the infection site, was not supported by the data. The immune response was explored using parameters for each immune state. The phagocytosis rate in neutropenic conditions, IR_{neu}, was not differentiable from k_{growth}, and was therefore fixed to 0, while k_{growth} was estimated at 0.372 h^{-1}. The phagocytosis rate in intermediate and immunocompetent conditions was estimated at 0.185 and 0.318 h^{-1}, respectively. The digestion rate k_{dig} was not significantly different from k_{phag}.

Bacterial counts (Fig. 3) were lower overall in control and treatment groups for immunocompetent conditions. However, the contribution of meropenem to bacterial killing was dependent on the immune status, with reduced meropenem-related bacterial killing in intermediate and immunocompetent groups. For example, the median decrease in CFU at 26 h in the 300 mg/kg q4h group compared to controls was ~4 $\log_{10}$ CFU in neutropenic mice versus ~2 $\log_{10}$ CFU in immunocompetent mice. The model fit was better (ΔOFV = −15.7) when the plasma concentration-time profile, rather than the ELF concentration-time profile, was driving the bacterial killing due to meropenem. Power and E_{max} models showed similar performances (ΔOFV = −1.8 for the E_{max} model). The E_{max} model was selected (Table 1) for biological plausibility and interpretability. The final model could capture observed bacterial counts across dose groups and immune states (Fig. 4).

Simulated dose-ranging and dose-fractionation studies

As in the original data, a larger relative difference in 24-h bacterial count between doses was predicted in neutropenic mice compared to the other immune states (Fig. 5), indicating a reduced dose-response gradient in immunocompetent conditions (Fig. S3). Similarly, in dose-fractionation studies, although frequent administrations led to the lowest bacterial counts in all immune states, the difference in predicted bacterial

Downloaded from https://journals.asm.org/journal/aac on 17 August 2026 by 130.238.171.108.

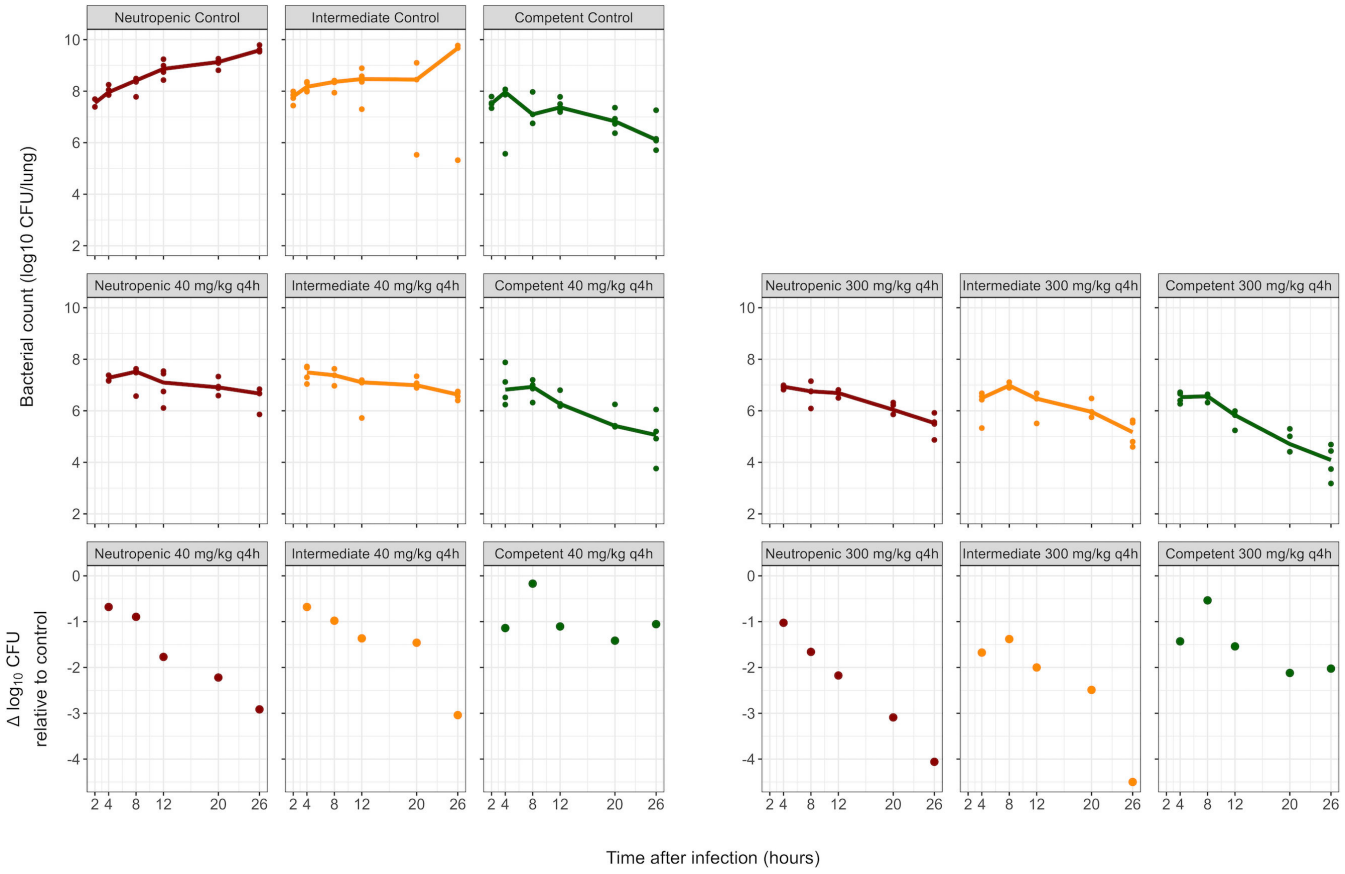

FIG 3 Bacterial counts measured in the PD experiments in neutropenic, intermediate suppression, and immunocompetent mice. Shown are observed (solid circles) and medians (solid lines) of bacterial counts in control groups (top row) and treatment groups (middle row). The bottom row depicts the differences in bacterial counts (in $\log_{10}$ CFU/lung) between median bacterial counts in treatment groups and median bacterial counts in control groups for the corresponding times and immune states.

killing between q2h administrations and other administration intervals was greater in neutropenic mice. The lowest doses or longest dosing intervals (e.g., 20 mg/kg q4h and 80 mg/kg q8h), predicted to achieve growth or stasis in neutropenic mice, achieved net killing in intermediate and immunocompetent mice at 24 h. For the highest or most frequent doses (e.g. 1,200 mg/kg q4h and 150 mg/kg q2h), lower bacterial counts at 24 h were predicted in neutropenic mice compared to mice with intermediate suppression.

For all immune states, the PK/PD indices (Fig. 6) showed the highest correlations for $fT_{>MIC}$ with predicted bacterial counts after 24 h of treatment ($R^2 > 0.9$). The R^2 value of *f*AUC/MIC was nonetheless noticeably improved in immunocompetent conditions ($R^2 = 0.74$ and 0.31 in immunocompetent and neutropenic states, respectively). A near-maximal effect was reached at lower $fT_{>MIC}$ values in intermediate and immunocompetent compared to neutropenic conditions. However, the $\log_{10}$ decrease in bacterial counts, compared to controls, at high $fT_{>MIC}$ values was lower in immunocompetent compared to neutropenic conditions.

DISCUSSION

This study used a standardized *in vivo* mouse lung infection model (9), with varying levels of immunosuppression, to quantify the immune response's contribution to bacterial killing and its impact on the PKPD of meropenem over time via a PKPD model.

Observed meropenem plasma and ELF concentrations indicated different PK profiles depending on the immune status. Similar trends have earlier been observed for tedizolid

Downloaded from https://journals.asm.org/journal/aac on 17 August 2026 by 130.238.171.108.

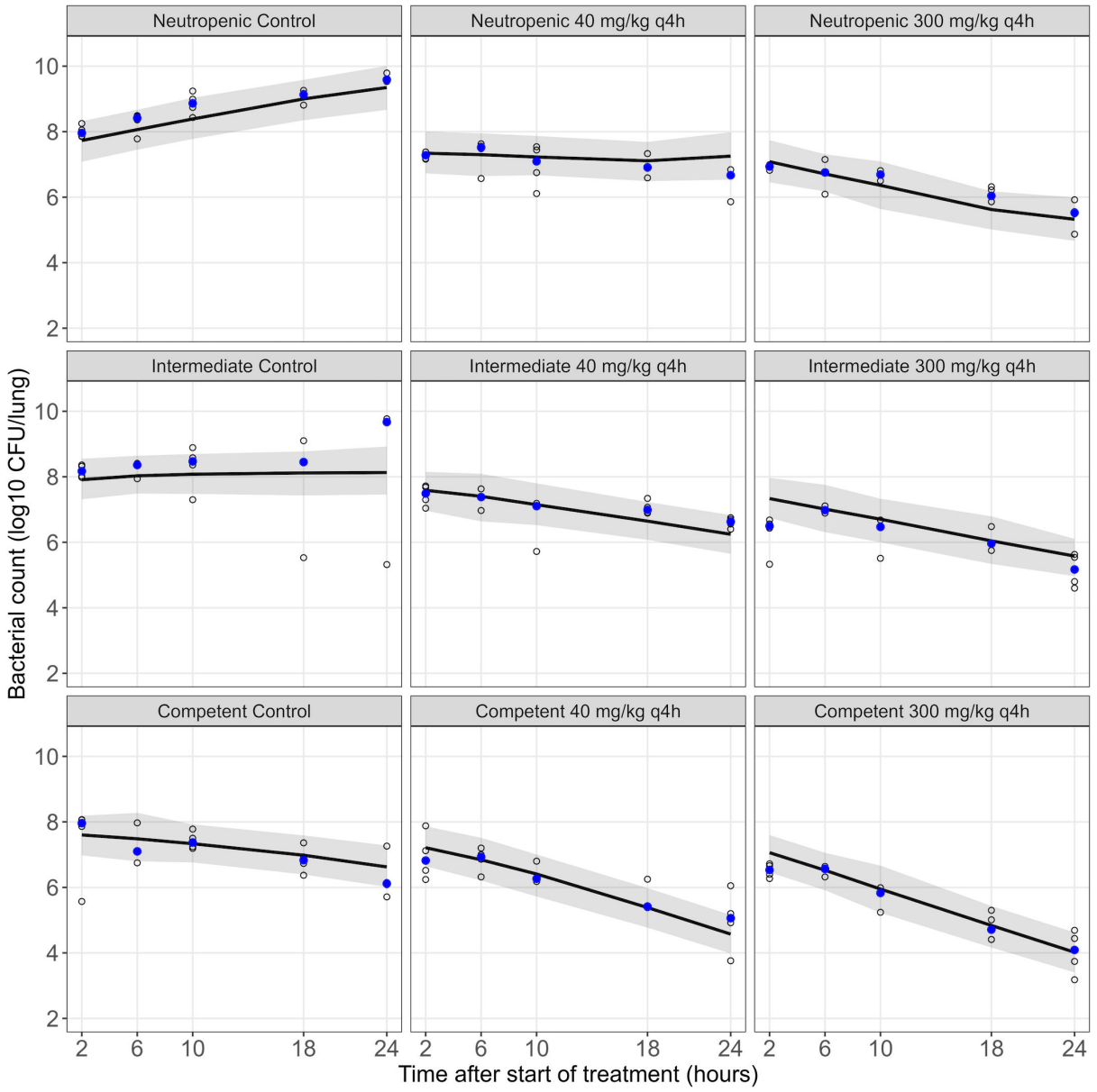

FIG 4 VPCs of the final PKPD model. Shown are the observed (open circles) and median of observed (solid blue circles) bacterial counts, the median (solid line) and 95% confidence interval of the median (shaded area) of model predictions for the meropenem dose groups in mice in a neutropenic, intermediate suppression, and immunocompetent state.

in ELF (37). A reduced volume of distribution in plasma in immunosuppressed mice could be due to cyclophosphamide affecting general well-being and fluid balance, or due to less meropenem being able to penetrate into immune cells (38). These findings highlight the importance of assessing antibiotic PK in the experimental conditions to be used in PKPD analyses.

The developed PKPD model described the immune response with an estimate of the apparent bacterial growth (accounting for immune response) in neutropenic mice, and a phagocytosis rate of 0.185 and 0.318 h^{-1} in intermediate and competent mice. Granulocyte dynamics could not be described, as blood counts showed no increase over 24 h, consistent with the multiple days required for neutrophil recovery after cyclophosphamide treatment (8). Furthermore, no delay and variations in immune response related to the neutrophil recruitment to the infection site could be characterized in the

Downloaded from https://journals.asm.org/journal/aac on 17 August 2026 by 130.238.171.108.

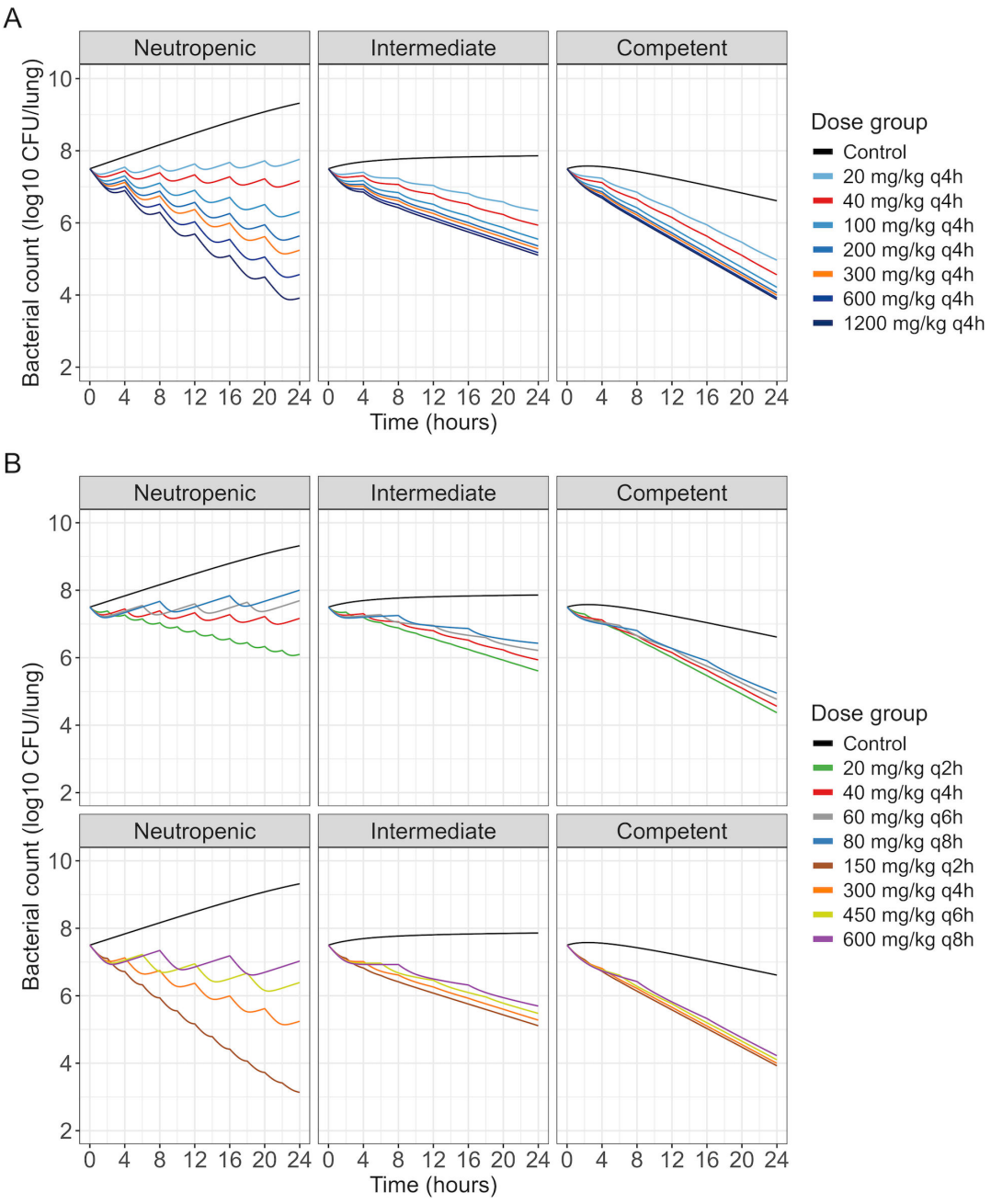

FIG 5 Predicted bacterial counts in mice in a neutropenic, intermediate suppression, or immunocompetent state based on the final PKPD model for (A) a dose-ranging study of meropenem and (B) a dose-fractionation study of meropenem (top row: fractionation of the first total dose, bottom row: fractionation of the second total dose).

PKPD model, as the time delay between the phagocytosis and digestion processes was sufficient to describe the observed data. In neutropenic conditions, the impact of the immune system was not differentiable from the bacterial growth rate. Additional data, such as experiments with different inoculum sizes, would be required to differentiate bacterial growth from the immune response in neutropenic conditions.

The contribution of meropenem to bacterial killing depended on the immune status, with a higher bacterial killing in neutropenic conditions compared to other immune states when comparing treatment and control groups. Similar behaviors were observed in the tedizolid dose-response in a neutropenic versus immunocompetent mouse

Downloaded from https://journals.asm.org/journal/aac on 17 August 2026 by 130.238.171.108.

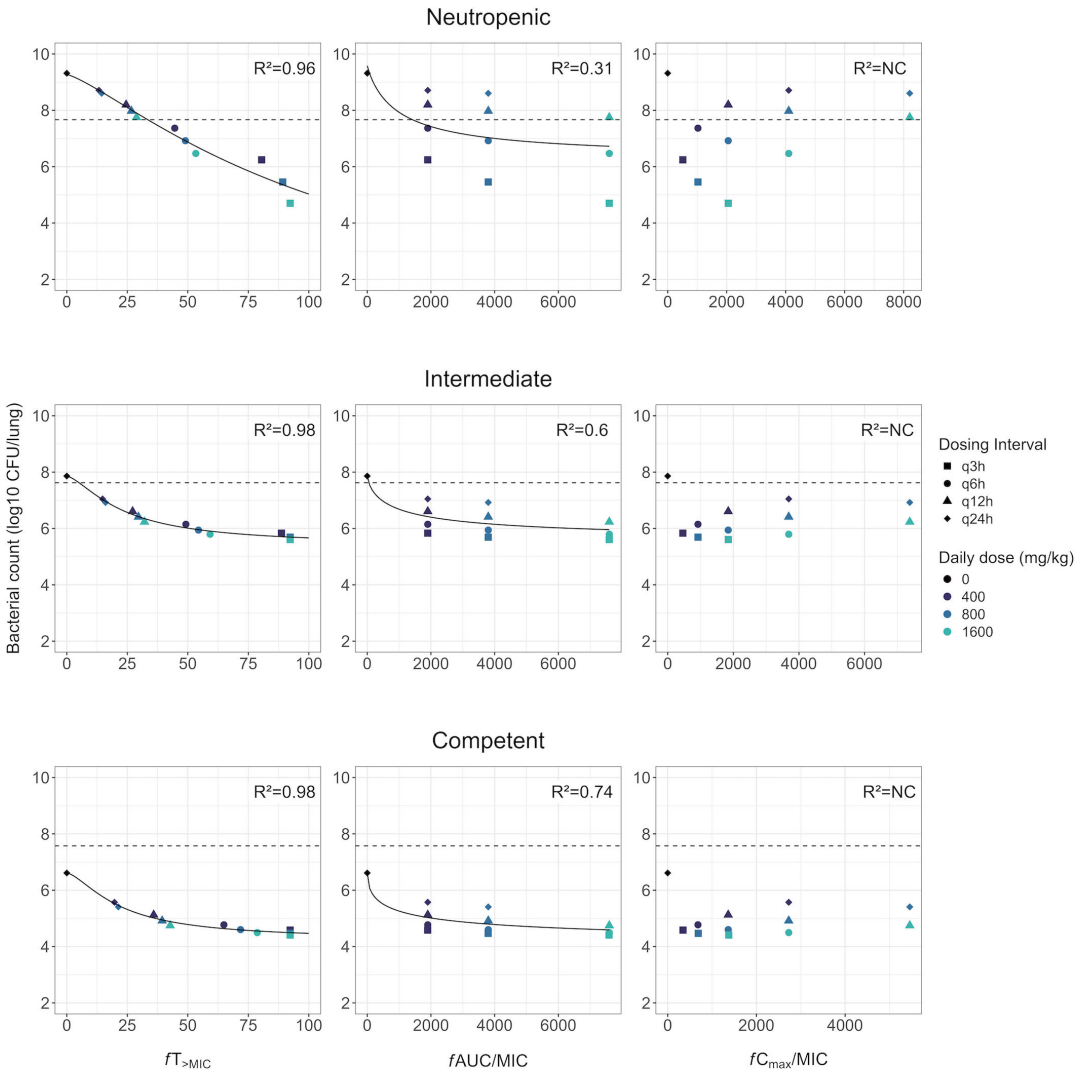

FIG 6 Relationship between plasma PK/PD indices and *K. pneumoniae* DSM116099 (MIC = 0.032 mg/L) bacterial counts at 26 h (24 h after start of treatment) in simulated meropenem dose-fractionation studies in mice in a neutropenic, intermediate immunosuppression, and immunocompetent state. Shown are the simulated bacterial counts (shapes), the stasis line (horizontal dashed line, corresponding to the bacterial count in control groups at 2 h after inoculation), the fitted E_{max} curve (solid line), and the R^2 value reported in each panel. NC, not computed.

thigh infection model (17). Nonetheless, there was no significant difference between immune states in the meropenem effect parameters. The observed differences were best explained by a higher proportion of the bacteria transferred to the P compartment in immunocompetent conditions, and thereby a lower fraction of the bacteria was exposed to meropenem in the S compartment. Consequently, although the internalized bacteria would eventually be cleared from the system, meropenem would be responsible for a lower reduction of CFU in immunocompetent conditions compared to neutropenic conditions. The data did not support an effect of meropenem within the immune cells. A lower intracellular activity of meropenem in monocytes, compared to extracellular conditions, has been shown *in vitro* (39).

In the simulated dose-ranging and fractionation studies, the dose-response gradient's dependence on immune status was illustrated. Bacterial counts were predicted to be at least as low in neutropenic conditions as in immunocompetent conditions for the highest doses or the most frequent administration schedule, while doses predicted to achieve stasis or growth in neutropenic conditions were predicted to achieve killing in immunocompetent conditions (Fig. 5).

Downloaded from https://journals.asm.org/journal/aac on 17 August 2026 by 130.238.171.108.

In dose-fractionation studies, frequent administrations were predicted to be the most effective for a given total dose, with $fT_{>MIC}$ identified as the PK/PD index with the highest correlation, as previously reported for meropenem (28, 40). Nonetheless, differences in bacterial counts compared to other dosing schedules were less apparent in immunocompetent conditions, impacting the predicted antibiotic efficacy for PK/PD index values. A near-maximal reduction of bacterial counts was achieved at $fT_{>MIC}$ ≈40% in immunocompetent mice, whereas an additional ~2 log decrease in counts was predicted when increasing $fT_{>MIC}$ from 40% to 80% in neutropenic mice. Derived efficacy targets would thus be expected to differ if performing a dose-fractionation study in a neutropenic or immunocompetent setting. It should be noted that for the studied strain, as bacterial counts in immunocompetent control groups were predicted below the stasis line at 26 h, targets would need to be tailored to other criteria than in neutropenic conditions. Overall, these results showed that conclusions drawn for antibiotic efficacy and dose selection could differ between the neutropenic and immunocompetent mouse infection models. Studies in immunocompetent mice could potentially provide insights into differences in efficacy between patient populations with different immune states, as well as improve the understanding of how different antibiotics depend on the immune system. As a perspective, *in vivo* studies with different types of immune deficiencies (using SCID, NOD, or gammac mouse models) may further inform how antibiotics and the immune system interact.

The developed model had some limitations. It was not possible to quantify a saturation of the immune response (14–16) based on available data, which would likely require expanded studies using several bacterial inoculum sizes. Furthermore, the group-dependent phagocytosis rate, in contrast to a continuous function, limits the capacity to extrapolate to unstudied conditions. As a single bacterial strain was studied, further explorations with other bacterial strains or species would be required to enhance the model's robustness.

In conclusion, the current study identified differences in meropenem PK between neutropenic and immunocompetent mouse infection models and quantified bacterial killing by the immune response and meropenem in a mouse lung infection model with varying degrees of immunosuppression. Meropenem was found to have a reduced contribution to bacterial killing in immunocompetent conditions, attributed to a lower fraction of bacteria affected by meropenem. Simulations demonstrated that outcomes of antibiotic PKPD analyses, such as PK/PD targets derived from PK/PD indices, will vary depending on the use of an immunocompetent or a neutropenic infection model.

ACKNOWLEDGMENTS

This project has received funding from the European Union's Horizon 2020 Research and Innovation Program under the Marie Skłodowska-Curie grant agreement number 861323 and the Swedish Research Council under grant number 2022-00657.

AUTHOR AFFILIATIONS

[1]Department of Pharmacy, Uppsala University, Uppsala, Sweden
[2]Division of Infectious Diseases, Paul-Ehrlich-Institut, Langen, Germany

AUTHOR ORCIDs

Raphaël Saporta https://orcid.org/0009-0005-3459-6839
Aghavni Ginosyan http://orcid.org/0009-0005-5546-6099
Irena Loryan http://orcid.org/0000-0002-1557-4416
Elisabet I. Nielsen http://orcid.org/0000-0003-0725-214X
Isabelle Bekeredjian-Ding http://orcid.org/0000-0001-6646-5888
Bernhard Kerscher http://orcid.org/0000-0001-9300-7401
Lena E. Friberg http://orcid.org/0000-0002-2979-679X

FUNDING

Funder	Grant(s)	Author(s)
H2020 Marie Skłodowska-Curie Actions	861323	Lena E. Friberg
Swedish Research Council	2022-00657	Lena E. Friberg

DATA AVAILABILITY

Data will be made available on request from the corresponding author.

ETHICS APPROVAL

All procedures were approved by the Hessian State Authority (approval number F107-2016, RP Darmstadt, Germany) and performed in accordance with institutional guidelines and the German animal laws.

ADDITIONAL FILES

The following material is available online.

Supplemental Material

Supplemental material (AAC01788-25-s0001.docx). Tables S1 and S2; Fig. S1 to S3.

REFERENCES

1. Chaplin DD. 2010. Overview of the immune response. J Allergy Clin Immunol 125:S3–S23. https://doi.org/10.1016/j.jaci.2009.12.980
2. Kolaczkowska E, Kubes P. 2013. Neutrophil recruitment and function in health and inflammation. Nat Rev Immunol 13:159–175. https://doi.org/10.1038/nri3399
3. Newburger PE, Dale DC. 2013. Evaluation and management of patients with isolated neutropenia. Semin Hematol 50:198–206. https://doi.org/10.1053/j.seminhematol.2013.06.010
4. Lyman GH, Michels SL, Reynolds MW, Barron R, Tomic KS, Yu J. 2010. Risk of mortality in patients with cancer who experience febrile neutropenia. Cancer 116:5555–5563. https://doi.org/10.1002/cncr.25332
5. EMA. 2018. Use of pharmacokinetics and pharmacodynamics in the development antibacterial medicinal products - Scientific guideline. Eur Med Agency. https://www.ema.europa.eu/en/use-pharmacokinetics-pharmacodynamics-development-antibacterial-medicinal-products-scientific.
6. Food and Drug Administration Center for Drug Evaluation and Research. 2017. Antibacterial therapies for patients with an unmet medical need for the treatment of serious bacterial diseases
7. Zhao M, Lepak AJ, Andes DR. 2016. Animal models in the pharmacokinetic/pharmacodynamic evaluation of antimicrobial agents. Bioorg Med Chem 24:6390–6400. https://doi.org/10.1016/j.bmc.2016.11.008
8. Zuluaga AF, Salazar BE, Rodriguez CA, Zapata AX, Agudelo M, Vesga O. 2006. Neutropenia induced in outbred mice by a simplified low-dose cyclophosphamide regimen: characterization and applicability to diverse experimental models of infectious diseases. BMC Infect Dis 6:55. https://doi.org/10.1186/1471-2334-6-55
9. Arrazuria R, Kerscher B, Huber KE, Hoover JL, Lundberg CV, Hansen JU, Sordello S, Renard S, Aranzana-Climent V, Hughes D, Gribbon P, Friberg LE, Bekeredjian-Ding I. 2022. Expert workshop summary: advancing toward a standardized murine model to evaluate treatments for antimicrobial resistance lung infections. Front Microbiol 13:988725. https://doi.org/10.3389/fmicb.2022.988725
10. Minichmayr IK, Aranzana-Climent V, Friberg LE. 2022. Pharmacokinetic/pharmacodynamic models for time courses of antibiotic effects. Int J Antimicrob Agents 60:106616. https://doi.org/10.1016/j.ijantimicag.2022.106616
11. Aranzana-Climent V, Hughes D, Cao S, Tomczak M, Urbas M, Zabicka D, Vingsbo Lundberg C, Hansen J, Lindberg J, Hobbie SN, Friberg LE. 2022. Translational *in vitro* and *in vivo* PKPD modelling for apramycin against Gram-negative lung pathogens to facilitate prediction of human efficacious dose in pneumonia. Clin Microbiol Infect 28:1367–1374. https://doi.org/10.1016/j.cmi.2022.05.003
12. Saporta R, Nielsen EI, Menetrey A, Cameron DR, Nicolas-Metral V, Friberg LE. 2024. Model-based translation of results from *in vitro* to *in vivo* experiments for afabicin activity against *Staphylococcus aureus*. J Antimicrob Chemother 79:3150–3159. https://doi.org/10.1093/jac/dkae334
13. Guo B, Abdelraouf K, Ledesma KR, Chang K-T, Nikolaou M, Tam VH. 2011. Quantitative impact of neutrophils on bacterial clearance in a murine pneumonia model. Antimicrob Agents Chemother 55:4601–4605. https://doi.org/10.1128/AAC.00508-11
14. Drusano GL, Fregeau C, Liu W, Brown DL, Louie A. 2010. Impact of burden on granulocyte clearance of bacteria in a mouse thigh infection model. Antimicrob Agents Chemother 54:4368–4372. https://doi.org/10.1128/AAC.00133-10
15. Drusano GL, VanScoy B, Liu W, Fikes S, Brown D, Louie A. 2011. Saturability of granulocyte kill of *Pseudomonas aeruginosa* in a murine model of pneumonia. Antimicrob Agents Chemother 55:2693–2695. https://doi.org/10.1128/AAC.01687-10
16. Thorsted A, Pham AD, Friberg LE, Nielsen EI. 2023. Model-based assessment of neutrophil-mediated phagocytosis and digestion of bacteria across *in vitro* and *in vivo* studies. CPT Pharmacometrics Syst Pharmacol 12:1972–1987. https://doi.org/10.1002/psp4.13046
17. Drusano GL, Liu W, Kulawy R, Louie A. 2011. Impact of granulocytes on the antimicrobial effect of tedizolid in a mouse thigh infection model. Antimicrob Agents Chemother 55:5300–5305. https://doi.org/10.1128/AAC.00502-11
18. Drusano GL, Liu W, Fikes S, Cirz R, Robbins N, Kurhanewicz S, Rodriquez J, Brown D, Baluya D, Louie A. 2014. Interaction of drug- and granulocyte-mediated killing of *Pseudomonas aeruginosa* in a murine pneumonia model. J Infect Dis 210:1319–1324. https://doi.org/10.1093/infdis/jiu237
19. Katsube T, Yamano Y, Yano Y. 2008. Pharmacokinetic-pharmacodynamic modeling and simulation for *in vivo* bactericidal effect in murine infection model. J Pharm Sci 97:1606–1614. https://doi.org/10.1002/jps.21062
20. Louie A, Liu W, VanGuilder M, Neely MN, Schumitzky A, Jelliffe R, Fikes S, Kurhanewicz S, Robbins N, Brown D, Baluya D, Drusano GL. 2015. Combination treatment with meropenem plus levofloxacin is synergistic against *Pseudomonas aeruginosa* infection in a murine model of pneumonia. J Infect Dis 211:1326–1333. https://doi.org/10.1093/infdis/jiu603
21. Papp-Wallace KM, Endimiani A, Taracila MA, Bonomo RA. 2011. Carbapenems: past, present, and future. Antimicrob Agents Chemother 55:4943–4960. https://doi.org/10.1128/AAC.00296-11

Downloaded from https://journals.asm.org/journal/aac on 17 August 2026 by 130.238.171.108.

22. European Committee for Antimicrobial Susceptibility Testing (EUCAST) of the European Society of Clinical Microbiology and Infectious Diseases (ESCMID). 2003. Determination of minimum inhibitory concentrations (MICs) of antibacterial agents by broth dilution. Clin Microbiol Infect 9:ix–xv. https://doi.org/10.1046/j.1469-0691.2003.00790.x
23. Decosterd LA, Mercier T, Ternon B, Cruchon S, Guignard N, Lahrichi S, Pesse B, Rochat B, Burger R, Lamoth F, Pagani J-L, Eggimann P, Csajka C, Choong E, Buclin T, Widmer N, André P, Marchetti O. 2020. Validation and clinical application of a multiplex high performance liquid chromatography – tandem mass spectrometry assay for the monitoring of plasma concentrations of 12 antibiotics in patients with severe bacterial infections. J Chromatogr B 1157:122160. https://doi.org/10.1016/j.jchromb.2020.122160
24. Parker SL, Pandey S, Sime FB, Lipman J, Roberts JA, Wallis SC. 2019. A validated LC-MSMS method for the simultaneous quantification of meropenem and vaborbactam in human plasma and renal replacement therapy effluent and its application to a pharmacokinetic study. Anal Bioanal Chem 411:7831–7840. https://doi.org/10.1007/s00216-019-02184-4
25. Huang L, Haagensen J, Verotta D, Lizak P, Aweeka F, Yang K. 2014. Determination of meropenem in bacterial media by LC–MS/MS. J Chromatogr B 961:71–76. https://doi.org/10.1016/j.jchromb.2014.05.002
26. Food and Drug Administration Center for Drug Evaluation and Research. 2022. M10 bioanalytical method validation and study sample analysis
27. Nielsen EI, Viberg A, Löwdin E, Cars O, Karlsson MO, Sandström M. 2007. Semimechanistic pharmacokinetic/pharmacodynamic model for assessment of activity of antibacterial agents from time-kill curve experiments. Antimicrob Agents Chemother 51:128–136. https://doi.org/10.1128/AAC.00604-06
28. Sugihara K, Sugihara C, Matsushita Y, Yamamura N, Uemori M, Tokumitsu A, Inoue H, Kakuta M, Namba E, Nasu H, Koga T. 2010. *In vivo* pharmacodynamic activity of tomopenem (formerly CS-023) against *Pseudomonas aeruginosa* and methicillin-resistant *Staphylococcus aureus* in a murine thigh infection model. Antimicrob Agents Chemother 54:5298–5302. https://doi.org/10.1128/AAC.00267-10
29. Beal S, Sheiner L, Boeckmann A, Bauer R. 1989. NONMEM 7.5 users guides. ICON plc, Gaithersburg, MD.
30. Keizer R, Karlsson M, Hooker A. 2013. Modeling and simulation workbench for NONMEM: tutorial on Pirana, PsN, and Xpose. CPT Pharmacomet Syst Pharmacol 2:1–9. https://doi.org/10.1038/psp.2013.24
31. Beal SL. 2001. Ways to fit a PK model with some data below the quantification limit. J Pharmacokinet Pharmacodyn 28:481–504. https://doi.org/10.1023/a:1012299115260
32. Dosne A-G, Bergstrand M, Harling K, Karlsson MO. 2016. Improving the estimation of parameter uncertainty distributions in nonlinear mixed effects models using sampling importance resampling. J Pharmacokinet Pharmacodyn 43:583–596. https://doi.org/10.1007/s10928-016-9487-8
33. Nguyen THT, Mouksassi M-S, Holford N, Al-Huniti N, Freedman I, Hooker AC, John J, Karlsson MO, Mould DR, Pérez Ruixo JJ, Plan EL, Savic R, van Hasselt JGC, Weber B, Zhou C, Comets E, Mentré F, Model Evaluation Group of the International Society of Pharmacometrics (ISoP) Best Practice Committee. 2017. Model evaluation of continuous data pharmacometric models: metrics and graphics. CPT Pharmacometrics Syst Pharmacol 6:87–109. https://doi.org/10.1002/psp4.12161
34. R Core Team. 2022. R: a language and environment for statistical computing. R Foundation for Statistical Computing, Vienna, Austria.
35. Baron K. 2023. mrgsolve: simulate from ODE-based models. R package.
36. Ritz C, Baty F, Streibig JC, Gerhard D. 2015. Dose-response analysis using R. PLoS One 10:e0146021. https://doi.org/10.1371/journal.pone.0146021
37. Abdelraouf K, Nicolau DP. 2017. Comparative *in vivo* efficacies of tedizolid in neutropenic versus immunocompetent murine *Streptococcus pneumoniae* lung infection models. Antimicrob Agents Chemother 61:e01957-16. https://doi.org/10.1128/AAC.01957-16
38. Van Bambeke F, Barcia-Macay M, Lemaire S, Tulkens PM. 2006. Cellular pharmacodynamics and pharmacokinetics of antibiotics: current views and perspectives. Curr Opin Drug Discov Devel 9:218–230.
39. Buyck JM, Tulkens PM, Van Bambeke F. 2013. Pharmacodynamic evaluation of the intracellular activity of antibiotics towards *Pseudomonas aeruginosa* PAO1 in a model of THP-1 human monocytes. Antimicrob Agents Chemother 57:2310–2318. https://doi.org/10.1128/AAC.02609-12
40. Nicolau DP. 2008. Pharmacokinetic and pharmacodynamic properties of meropenem. Clin Infect Dis 47 Suppl 1:S32–S40. https://doi.org/10.1086/590064

Downloaded from https://journals.asm.org/journal/aac on 17 August 2026 by 130.238.171.108.